International Journal of Heat and Technology
Vol. 43, No. 6, December, 2025, pp. 2424-2438
Journal homepage: http://iieta.org/journals/ijht

Simulation-Based Analysis of the Thermal Regulation Effects of Traditional Skywell Layouts in Modern Relocation Projects

Zhiming Peng[1], Hu Wang[2*], Tengxiang Zhong[3], Jingyi Shao[3], Leqi Li[3]

[1] School of Architecture and Civil Engineering, Huangshan University, Huangshan 245041, China
[2] Anhui Jianzhu University Design & Research Institute Co., Ltd., Hefei 230601, China
[3] School of Architecture and Urban Planning, Anhui Jianzhu University, Hefei 230601, China

Corresponding Author Email: wh13956022885@sina.com

https://doi.org/10.18280/ijht.430638

Received: 16 May 2025
Revised: 10 November 2025
Accepted: 25 November 2025
Available online: 31 December 2025

Keywords:
traditional skywell, modern relocation, thermal environment regulation, thermodynamic constraints, conditional generative adversarial network (cGAN)

ABSTRACT

Traditional skywells, relying on the coupled thermodynamic mechanisms of natural ventilation, heat storage and release, and radiative heat transfer, exhibit outstanding passive thermal regulation capabilities and offer valuable references for low-energy building design. However, during modern relocation projects, increasing conflicts emerge between traditional skywell morphologies and contemporary thermal performance requirements as well as urban spatial constraints. Conventional forward design approaches based on iterative "parameter adjustment–simulation validation" are often inefficient and fail to ensure precise thermodynamic performance matching, thereby limiting the scientific rigor and feasibility of relocation practices. To address the coordinated challenge of traditional form preservation, thermodynamic performance optimization, and relocation scenario adaptability, this study aims to quantitatively evaluate and optimize the thermal regulation effects of skywells after relocation. A thermodynamically constrained conditional generative adversarial network (cGAN)–based inverse generation framework is proposed, overcoming the limitations of traditional forward workflows and enabling efficient back-propagation from target thermal environment indicators to optimal skywell design parameters. Using representative traditional skywell relocation projects as case studies, a comprehensive analytical framework is established, integrating thermodynamic mechanism analysis, inverse generative optimization, and performance verification. The framework systematically covers multiple relocation scenarios, including single-building relocation, clustered relocation, and cross-climatic relocation. The results demonstrate that the proposed model achieves highly efficient and accurate optimization of thermal environments in relocated traditional skywells. Compared with conventional forward design methods, the computational time per design scheme is reduced by 99.3%, while the prediction errors of temperature and heat flux are limited to 2.1% and 3.2%, respectively. Across the three typical relocation scenarios, the optimized solutions exhibit consistently superior performance: unit-area heat loss is reduced by 22.2% in single-building relocation, thermal storage efficiency increases by 13 percentage points in cross-climatic relocation, and all generated schemes achieve a 100% compliance rate in terms of traditional morphological compatibility. This study provides a thermodynamically guided and data-driven optimization pathway for the thermal environment design of relocated traditional skywells, enriching the methodological framework for adaptive reuse of architectural heritage and offering critical technical support for traditional building relocation projects in the context of low-carbon urban development.

1. INTRODUCTION

Under the background of global low-carbon transition and architectural heritage conservation, the passive thermal regulation wisdom of traditional buildings has become an important reference for modern low-energy building design [1-3]. As a typical passive spatial form, the traditional skywell dynamically regulates the indoor thermal environment through the coupled effects of natural ventilation, heat storage and release, and radiative heat transfer [4, 5]. Its core thermodynamic mechanisms are manifested as buoyancy-driven air circulation enhancing heat exchange, sensible heat storage and release of the building envelope regulating temperature fluctuations, and the radiative characteristics of roofs and walls optimizing the utilization of solar radiation. This regulation mode without active energy input shows significant advantages in reducing energy consumption and improving thermal comfort, providing an important technical prototype for modern low-energy buildings [6, 7]. However, during the modern relocation of traditional skywells, significant adaptation conflicts exist between the original thermal regulation mechanisms and relocation scenarios.

Urban space scarcity restricts skywell dimensions, damaging ventilation paths and buoyancy conditions [8]; cross-climatic relocation exposes skywells to entirely new temperature, humidity, and radiation environments, causing the original regulation strategies to fail; the superposition of urban heat island effects and surrounding obstructions interferes with radiative heat exchange and ventilation efficiency; and the replacement of traditional materials directly alters thermodynamic parameters, weakening heat storage and release capacity. These factors lead to a substantial degradation of thermal regulation performance after relocation, resulting in a prominent imbalance between traditional form and modern thermal demands, which constrains the adaptive reuse of architectural heritage [9, 10]. Accurately simulating and optimizing the thermal environment regulation effects of relocated skywells is key to achieving the synergy between architectural heritage activation and low-carbon urban development. However, current experience-based design and forward trial-and-error methods struggle to precisely capture complex thermodynamic mechanisms and fail to efficiently balance form preservation and performance optimization. There is an urgent need for thermodynamically guided innovative design methods to provide scientific support, with both important academic value and engineering practical significance.

Thermal environment simulation of traditional buildings mainly relies on forward analysis methods. Computational fluid dynamics simulations have become a mainstream tool due to their ability to finely characterize thermal flow fields and are widely used in quantitative studies of the influence of geometric parameters on thermal environments [11]. Surrogate models improve computational efficiency by fitting high-fidelity data through machine learning, providing possibilities for multi-parameter optimization [12-14]. However, these forward methods are essentially trial-and-error processes of parameter adjustment and simulation validation, and they exhibit clear limitations in relocation scenarios. Faced with complex combinations of multi-parameter coupling, dynamic climates, and spatial constraints, they require a large number of iterative computations, resulting in low efficiency [15]. Moreover, these models rely on data fitting and lack constraints from thermodynamic conservation laws. In data-scarce regions such as extreme parameters or new relocation scenarios, their prediction results have insufficient physical credibility, making it difficult to ensure the stability of design solutions [16, 17]. Inverse design methods provide a new pathway to address this problem. Generative models such as generative adversarial networks have gradually been applied to architectural design due to their strong mapping capabilities and have achieved breakthroughs in inferring design solutions from target performance, significantly improving efficiency [18, 19]. However, existing studies have evident gaps. Most focus on general forms of modern buildings and ignore traditional architectural form constraints, which can easily damage cultural characteristics. More critically, they lack deep integration of the core thermodynamic mechanisms of thermal regulation, and the generated solutions may violate basic principles such as energy conservation and heat flux continuity, leading to large deviations between actual performance and predictions, and failing to meet the requirements of precise design for relocation projects. In recent years, physics-informed generative models have become a research frontier. By embedding physical equations, these models improve the physical credibility of generated results. Related studies have embedded fluid dynamics and energy equations into generative adversarial networks and applied them to heat conduction problems [20]. However, most focus on general thermodynamic problems and do not construct customized constraints for the ventilation–heat storage–radiation coupling mechanisms specific to traditional skywells. Meanwhile, how to coordinately embed morphological, environmental, and thermodynamic constraints for relocation scenarios to achieve precise inverse inference from target thermal environments to adaptive design solutions remains a research gap, providing a clear academic entry point for this study.

The core objectives of this study are threefold: to construct a cGAN inverse model integrating the thermal regulation mechanisms of traditional skywells, achieving deep coupling between thermodynamic constraints and generative models; to accurately simulate and quantitatively evaluate the thermal environment regulation effects of skywells under different relocation scenarios, revealing the influence patterns of relocation factors on thermodynamic performance; and to propose efficient thermal environment optimization design solutions for relocation scenarios, achieving coordination between traditional form preservation and modern thermal demands. The main innovations are as follows:

First, the ventilation–heat storage–radiation coupled thermodynamic mechanisms specific to traditional skywells are embedded into the loss function of a cGAN for the first time. Thermodynamic consistency constraints are constructed by introducing energy conservation residuals, heat flux continuity residuals, and thermal mass temperature deviation terms, ensuring the physical credibility and performance stability of generated solutions.

Second, an inverse design framework that coordinates target thermal environments, traditional forms, and relocation constraints is established, breaking the efficiency bottleneck of forward methods and enabling direct inference from target thermal performance to design parameters, balancing form inheritance and performance optimization.

Third, a multi-scenario quantitative analysis framework covering single-building relocation, clustered relocation, and cross-climatic relocation is constructed to systematically analyze the thermodynamic response patterns of skywells under different scenarios, enhancing the general applicability and engineering value of the results.

The subsequent structure of this paper is organized as follows. Chapter 3 systematically elaborates the core thermodynamic mechanisms of thermal regulation in traditional skywells, constructs a cGAN architecture incorporating thermodynamic constraints, clarifies the methods for high-fidelity simulation and training data construction, and establishes a quantitative indicator system for thermal environment regulation effects under relocation scenarios. Chapter 4 designs multi-scenario relocation cases and comparative experiments, completes model training and performance evaluation, and verifies the superiority of the proposed method. Chapter 5 presents and analyzes the simulation results for different relocation scenarios and discusses the thermodynamic advantage mechanisms of the design solutions. Chapter 6 summarizes the main conclusions, elaborates the academic contributions and engineering significance, and proposes future research directions. The technical route of this study follows the logic of mechanism analysis–data construction–model training–case verification–conclusion and outlook. First, theoretical analysis and field

investigation are used to analyze the coupled thermal regulation mechanisms of skywells and determine the core thermodynamic equations and parameters. Then, based on orthogonal experimental design parameter ranges, high-fidelity computational fluid dynamics simulations are conducted to obtain paired samples of design parameters and thermal environment data, constructing and validating the training dataset. Subsequently, thermodynamic constraints are embedded to construct the model and complete training and evaluation. Optimization solutions are generated for multiple relocation scenarios, and thermal environment regulation effects are verified through simulation and field monitoring. Finally, conclusions are summarized and expansion directions are proposed. The key thermodynamic indicators throughout the process include ventilation heat replacement efficiency, heat storage efficiency, heat flux loss, and extreme climate thermal resilience, while the core methods include thermodynamic mechanism modeling, cGAN training, high-fidelity computational fluid dynamics simulation, and multi-scenario comparative validation.

2. THEORETICAL BASIS AND METHODOLOGICAL FRAMEWORK

2.1 Core thermodynamic mechanisms of thermal regulation in traditional skywells

The thermal regulation effect of traditional skywells originates from the coupled action of natural ventilation heat convection, heat storage and release of the building envelope, and solar radiative heat transfer. These mechanisms act synergistically to form a dynamic thermal balance system. Natural ventilation is dominated by buoyancy-driven flow. The air density difference between the skywell and indoor space generates a buoyancy pressure difference, and its core equation can be expressed as:

$$\Delta P=\rho_0 gH\left(\frac{1}{T_0}-\frac{1}{T_i}\right) \tag{1}$$

where, ΔP is the buoyancy pressure difference, ρ_0 is the outdoor air density, g is the gravitational acceleration, H is the effective height of the skywell, and T_0 and T_i are the average outdoor and indoor temperatures, respectively. Based on this, the air circulation process is accompanied by enthalpy change transfer, and the enthalpy change equation is:

$$\Delta h=c_p\Delta T \tag{2}$$

where, c_p is the specific heat capacity of air at constant pressure, and ΔT is the temperature difference between inlet and outlet air. Accordingly, the ventilation heat exchange efficiency can be defined as:

$$\eta_v=\frac{m_a c_p\Delta T}{Q_s} \tag{3}$$

where, m_a is the ventilation mass flow rate and Q_s is the total indoor heat gain, which is used to quantify the contribution of ventilation to indoor thermal environment regulation. The heat storage and release process of the building envelope follows Fourier's law of heat conduction and the principle of energy balance. Fourier's law is expressed as:

$$q=-\lambda\frac{\partial T}{\partial n} \tag{4}$$

where, λ is the thermal conductivity of the material, and $\partial T/\partial n$ is the temperature gradient. Combined with energy balance, a heat storage model is established, and the heat storage efficiency is defined as:

$$\eta_s=\frac{Q_{store}}{Q_{in}} \tag{5}$$

where, Q_{store} is the heat stored in the thermal mass and Q_{in} is the incoming heat. Meanwhile, a temperature attenuation coefficient β is introduced to describe the attenuation degree of temperature fluctuations in the thermal mass, enabling quantitative comparison of the heat storage performance between traditional masonry and timber materials and modern replacement materials. The solar radiative heat transfer mechanism is realized by constructing a radiative heat transfer model for the skywell roof and walls, considering the combined effects of solar short-wave radiation absorption and long-wave radiation emission. The radiative heat transfer coefficient can be derived as:

$$h_r=\frac{\varepsilon\sigma(T_s^4-T_a^4)}{T_s-T_a} \tag{6}$$

where, ε is the surface emissivity, σ is the Stefan–Boltzmann constant, and T_s and T_a are the surface temperature of the building envelope and the ambient temperature, respectively. This coefficient directly reflects the influence intensity of radiative heat transfer on the indoor thermal environment.

Relocation scenarios significantly alter the thermodynamic boundary conditions of the above mechanisms. Compared with the original context, the outdoor temperature baseline after relocation increases due to the urban heat island effect, solar radiation is attenuated by surrounding building shading, and wind speed and wind direction distributions change due to adjustments in urban morphology. These parameter changes jointly lead to the reconstruction of buoyancy-driven capacity, the amplitude of thermal mass temperature fluctuations, and radiative heat transfer intensity, ultimately affecting the performance of skywell thermal regulation. Therefore, it is necessary to clarify the influence patterns of boundary condition changes on thermal regulation mechanisms through quantitative comparison.

2.2 Construction of the thermodynamically constrained cGAN inverse generation model

2.2.1 Overall model architecture

The thermodynamically constrained cGAN inverse generation model takes "constraint embedding–inverse mapping–adversarial validation" as its core logic. It adopts a dual-network adversarial cooperative structure consisting of a generator G and a discriminator D, explicitly defining the network parameters and gradient update strategies of each module, to achieve accurate inverse inference from target thermal environments to compliant skywell design parameters. Figure 1 shows the overall architecture of the model.

The generator adopts a three-stage structure of "feature encoding–core mapping–parameter decoding". The input layer receives a fused feature vector with a dimension of $D_{in}=3N$, where N represents the number of quantitative indicators

for a single type of constraint. The feature vector consists of N_1-dimensional target thermal environment indicators, N_2-dimensional thermodynamic constraint parameters, and N_3-dimensional traditional morphological constraint parameters, satisfying the dimensional balance condition $N_1 + N_2 + N_3 = 3N$. The feature encoding stage adopts a three-layer convolutional structure, using 3 × 3 convolution kernels with a stride of 2. The activation function is LeakyReLU combined with batch normalization. Through this series of designs, the input feature dimension is compressed to $D_{mid} = N/4$. The core mapping layer consists of two fully connected layers, with the number of hidden neurons set to $2D_{mid}$. The GELU activation function is used to enhance the nonlinear representation capability of feature transformation. The parameter decoding stage also adopts a three-layer deconvolution structure, maintaining the configuration of 3 × 3 convolution kernels and stride 2, with ReLU as the activation function. The final output dimension is $D_{out} = M + C \times H \times W$. Here, M denotes the number of skywell design parameters, and $C \times H \times W$ corresponds to the feature map dimensions of the predicted thermal environment distribution. C is set to 3, corresponding to the temperature field, heat flux field, and wind velocity field, respectively, while H and W represent the spatial resolution. The discriminator adopts a PatchGAN structure. The input is the coupled feature of "design parameters–thermal environment distribution", whose dimension is consistent with the generator output, namely $M + C \times H \times W$. The feature extraction stage of the discriminator adopts a four-layer convolutional structure, with a convolution kernel size of 4 × 4 and a stride of 2. The activation function is LeakyReLU combined with batch normalization. After extracting local features through this structure, a convolutional layer with a Sigmoid activation function outputs an authenticity score map with a dimension of $S \times S$, where $S = H/16$. Meanwhile, the discriminator embeds a thermodynamic verification sub-network, which outputs a thermodynamic consistency score with a dimension of 1, realizing dual validation of the generated results. The model training adopts an alternating iterative strategy. The objective function of the discriminator is to minimize the classification error between real samples and generated samples, expressed as:

$$L_D = -E_{(x,y)\sim p_{data}}[\log D(x,y)] - E_{z\sim p_z}[\log(1 - D(G(z),\hat{y}))] \quad (7)$$

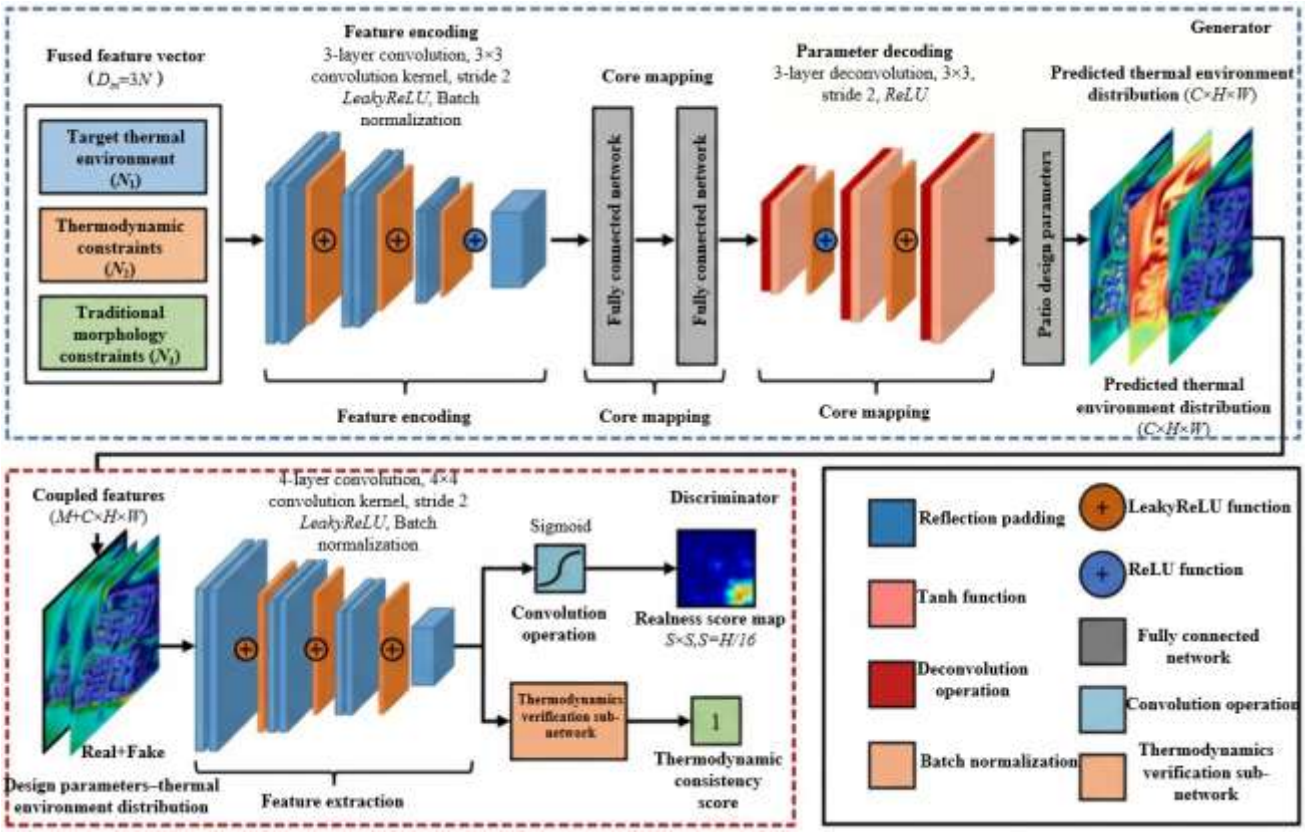

Figure 1. Overall model architecture

The objective function of the generator is to maximize the discriminator's misclassification probability of generated samples while minimizing the deviation between the predicted thermal environment and the target, expressed as:

$$L_G = -E_{z\sim p_z}[\log D(G(z),\hat{y})] + \alpha\|\hat{y} - y_{target}\|_1 \quad (8)$$

where, x denotes the real design parameters, y denotes the real thermal environment distribution, z denotes the input fused feature, $\hat{y}$ denotes the predicted thermal environment distribution, y_{target} denotes the target thermal environment indicators, and α is the reconstruction loss weight. Through adversarial training, the generator gradually learns an accurate mapping of "constraints–design–performance", while the discriminator realizes dual validation of the authenticity and thermodynamic rationality of the generated results.

2.2.2 Key module design

The key module design takes deep embedding of thermodynamic mechanisms as the core innovation. Through refined feature engineering and network structure design, it ensures the accuracy of constraint transmission and the

effectiveness of feature extraction. The input layer adopts a two-step processing strategy of "quantitative normalization–feature fusion". The target thermal environment indicator system selects core thermodynamic parameters such as summer maximum temperature T_{max}, unit-area heat flux loss q_{loss}, and ventilation heat replacement efficiency η_v. Their quantitative ranges are $T_{max} \in [25,32]$℃, $q_{loss} \in [0,30]$ W/m², and $\eta_v \in [0.4,0.8]$, respectively. Thermodynamic constraints are defined through quantitative thresholds, with energy conservation residual $\Delta E \leq 10^{-3}$ J and heat flux continuity residual $\Delta q \leq 5$ W/m². Traditional morphological constraints adopt interval quantification, including aspect ratio $AR \in [1.0,2.0]$, opening ratio $OR \in [0.3,0.6]$, and proportion of traditional components $R_c \in [0.4,1.0]$. All input parameters are processed by min–max normalization, and cross-dimensional fusion is achieved through a feature fusion matrix. The fusion formula is:

$$z=W_1 z_{thermal}+W_2 z_{constraint}+W_3 z_{morphology} \tag{9}$$

where, $z_{thermal}$, $z_{constraint}$, and $z_{morphology}$ are the normalized feature vectors of the target thermal environment, thermodynamic constraints, and traditional morphology, respectively. W_1, W_2, and W_3 are learnable fusion weight matrices with dimensions of $3N \times 3N$, which adaptively adjust the contribution weights of each feature through training. Figure 2 intuitively illustrates the input-layer feature fusion process. The generator adopts an improved U-Net architecture. A thermodynamic feature extraction module is added between the encoding and decoding ends. This module consists of two dedicated convolutional layers. The kernel parameters of the first layer are optimized based on the buoyancy pressure difference equation and the heat storage model, expressed as:

$$k_1=\frac{1}{H}\cdot\nabla\left(\rho_0 g\left(\frac{1}{T_0}-\frac{1}{T_i}\right)\right) \tag{10}$$

which, specifically extracts coupled features of skywell geometric parameters and buoyancy pressure difference. The kernel parameters of the second convolutional layer are optimized based on Fourier's law, expressed as:

$$k_2=\lambda\cdot\nabla\left(\frac{\partial T}{\partial n}\right) \tag{11}$$

which, focuses on extracting the correlation features between material parameters and heat flux. The encoding end uses downsampling convolutions to gradually compress the feature map size, while the decoding end uses transposed convolutions to restore the size. Meanwhile, skip connections are used to fuse the thermodynamic features from the encoding end with the features of the decoding end, enhancing the thermodynamic relevance of the generated parameters. The discriminator adopts a dual-branch parallel structure of "main branch–thermodynamic branch". The main branch realizes local authenticity discrimination through PatchGAN, while the thermodynamic branch embeds the energy conservation equation, heat flux continuity equation, and heat storage model derived in Section 3.1. It performs pixel-wise verification on the input thermal environment distribution feature maps and outputs a thermodynamic consistency score S_{thermo}. The final comprehensive score is obtained through weighted fusion:

$$S_{total}=\gamma S_{real}+(1-\gamma)S_{thermo} \tag{12}$$

where, S_{real} is the authenticity score and $\gamma = 0.6$ is the weighting coefficient, achieving dual constraints and accurate evaluation of the generated results.

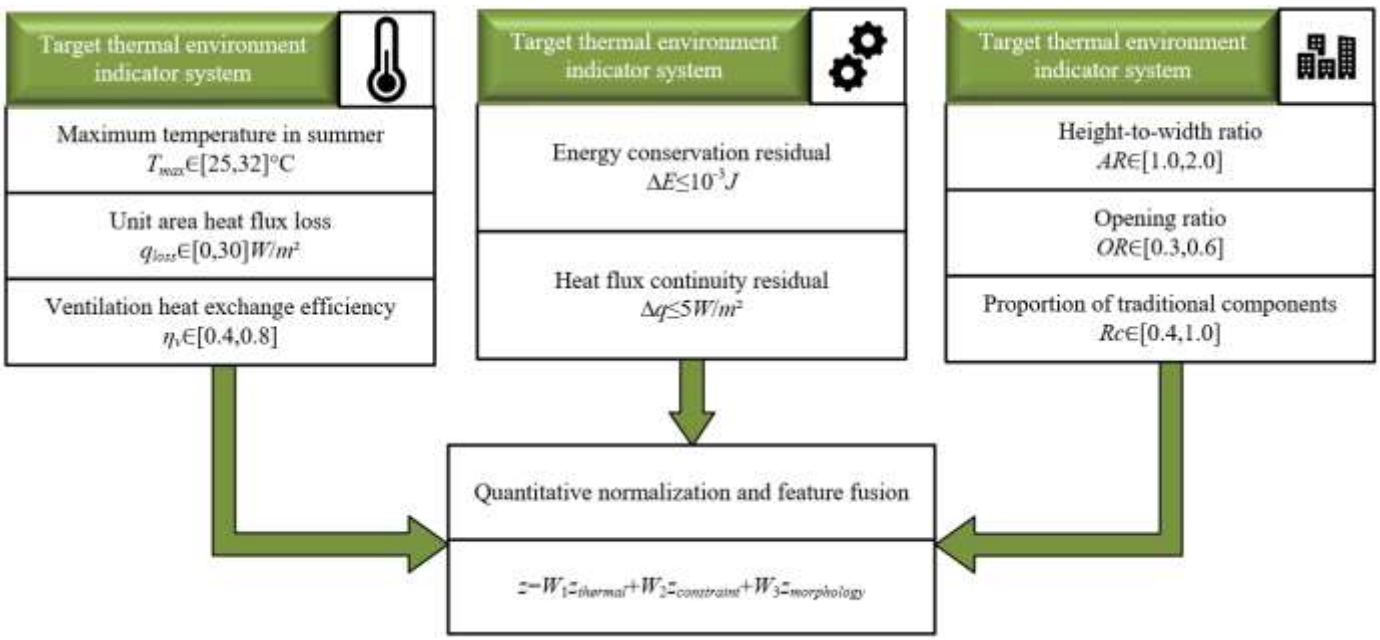

Figure 2. Schematic diagram of the input-layer feature fusion process

2.2.3 Construction of the loss function integrating thermodynamic constraints

Based on the dual-network adversarial architecture and the thermodynamic feature embedding design, a collaborative optimization objective function of "adversarial loss–reconstruction loss–thermodynamic consistency loss" is constructed. This ensures that model training not only approaches the real sample distribution but also strictly follows thermodynamic laws, while adapting to the input feature fusion and dual-branch discrimination logic. The core

expression is optimized as:

$$Loss_{total}=Loss_{adv}+\alpha\cdot Loss_{rec}+\beta\cdot Loss_{thermo} \quad (13)$$

where, α is the reconstruction loss weight, with a range of $\alpha \in [1.0,3.0]$, and $\beta$is the thermodynamic consistency loss weight, with a range of $\beta \in [2.0,5.0]$. The weight ratio balances the priority between "authenticity fitting" and "physical law constraints".

The adversarial loss $Loss_{adv}$ adopts the Wasserstein distance form in Section 2.2.1 and is adapted to the local authenticity scoring logic of the PatchGAN discriminator. The expression is:

$$Loss_{adv}=E_{(x,y)\sim p_{data}}[D_{total}(x,y)]-E_{z\sim p_z}[D_{total}(G(z),\hat{y})] \quad (14)$$

where, $D_{total}(\ )$ is the comprehensive score of the dual-branch discriminator, defined as $D_{total}=\gamma S_{real}+(1-\gamma)S_{thermo}$. Through this form, the "authenticity score" and the "thermodynamic consistency score" are simultaneously incorporated into the adversarial game, enabling the generator training to directly respond to the dual-branch discrimination signals.

The reconstruction loss $Loss_{rec}$ is a weighted sum of "design parameter reconstruction loss + thermal environment distribution reconstruction loss", adapted to the generator output structure of "simultaneous output of design parameters and thermal environment distribution":

$$Loss_{rec}=\omega_1\cdot\|G_x(z)-x_{ref}\|_1+\omega_2\cdot\|G_y(z)-y_{target}\|_1 \quad (15)$$

where, $G_x(z)$ is the generated skywell design parameter set, x_{ref} is the real design parameter sample, $G_y(z)$ is the predicted thermal environment distribution, and y_{target} is the target thermal environment indicator. ω_1 and ω_2 are weighting coefficients, prioritizing the adaptability of the thermal environment distribution to the target while constraining the rationality of the design parameters. This form corresponds to the generator output dimension design in Section 2.2.1 and realizes accurate constraints on the dual outputs.

The thermodynamic consistency loss $Loss_{thermo}$ closely corresponds to the thermodynamic feature extraction module and constraint quantification indicators in Section 2.2.2 and is constructed based on the thermal regulation mechanisms of traditional skywells. The expression is:

$$Loss_{thermo}=\lambda_1\cdot\frac{|\Delta E|}{\Delta E_{th}}+\lambda_2\cdot\frac{|\Delta q|}{\Delta q_{th}}+\lambda_3\cdot\frac{|\Delta T_{store}|}{T_{th}} \quad (16)$$

where, ΔE is the energy conservation residual, $\Delta E_{th}=10^{-3}$ J is the energy conservation residual threshold defined in Section 2.2.2; Δq is the heat flux continuity residual, and $\Delta q_{th}=5\ \mathrm{W/m^2}$ is the heat flux continuity residual threshold in Section 3.2.2; ΔT_{store} is the temperature variation deviation of the thermal mass, and ΔT_{th} = 2℃ is the quantitative threshold adapted to the heat storage characteristics of traditional materials. Through normalization by "residual / threshold", the dimensions of each loss term are unified, avoiding excessive dominance of any single type of constraint. λ_1, λ_2, and λ_3 are sub-weights satisfying $\lambda_1+\lambda_2+\lambda_3=1$, which are determined through optimization using orthogonal experiments. The experimental levels are set in combination with the convolution kernel parameter ranges of the thermodynamic feature extraction module, ensuring coordination between the weight ratio and the feature extraction logic.

2.3 High-fidelity thermodynamic simulation and training data construction

High-fidelity thermodynamic simulation and training data construction constitute the foundation for ensuring the effectiveness of model training and physical credibility. The core objective is to generate high-quality paired samples of "design parameters–thermal environment data" through refined CFD simulations and systematic data processing. CFD simulations are implemented using the open-source software OpenFOAM. Geometric modeling is carried out based on parametric CAD tools to construct three-dimensional models of the traditional skywell and its surrounding environment. The model includes the main body of the skywell, adjacent rooms, and the outlines of surrounding buildings under relocation scenarios, ensuring consistency between the geometric form and actual relocation projects. Mesh generation adopts a hybrid strategy combining structured and unstructured grids. Grid refinement is applied to key heat-exchange regions such as the skywell opening, the interface between rooms and the skywell, and the surfaces of envelope structures. The grid size is controlled within 0.1–0.3 m, and the optimal mesh scheme is determined through grid independence verification. Thermodynamic boundary conditions are set based on typical meteorological year data of the relocation site obtained from field monitoring. Outdoor temperature, solar radiation, and wind speed are applied as time-varying boundary conditions. The envelope surfaces are defined as thermal boundaries coupled with radiation and convection, while constant heat sources are set indoors to simulate heat dissipation from occupants and equipment. The RNG k-ε turbulence model is selected as the solver, which provides higher accuracy in simulating thermal convection and turbulent diffusion in complex spaces. Together with the PISO algorithm, the continuity equation, momentum equations, and energy equation are solved. The time step is set to 0.01 s to ensure numerical stability and convergence. Figure 3 shows the simulation and training data construction process for the thermal environment of the traditional skywell.

The construction of the training dataset is based on orthogonal experimental design. The skywell height-to-width ratio, opening ratio, envelope material, and eave length are selected as key design parameters. Parameter ranges are determined with reference to traditional skywell morphological characteristics and relocation constraints. An *L*9 (3^4) orthogonal table is used to generate 81 representative design schemes. For each scheme, both steady-state and transient CFD simulations are conducted. Steady-state simulations output spatial distribution data of temperature fields, heat flux fields, and wind speed fields, while transient simulations output time-series data of thermal storage body temperature and ventilation heat exchange. Design parameter vectors and the corresponding thermal environment feature data are then extracted to form the initial paired sample set. Data preprocessing adopts a two-step approach. First, abnormal samples caused by non-convergent boundary condition iterations during simulations are removed using the 3σ criterion. Second, min–max normalization is applied to map all data to the [0,1] interval, eliminating the influence of

dimensional differences on model training. Data validation is completed through field measurements. Temperature and heat flux sensors are installed simultaneously at the original sites of traditional skywells and at relocation pilot areas. Time-series data are continuously monitored for 72 h. The measured data are quantitatively compared with CFD simulation results under corresponding conditions. The validation results show that temperature errors are less than 2.5% and heat flux errors are less than 4%, meeting the credibility requirements for thermodynamic data.

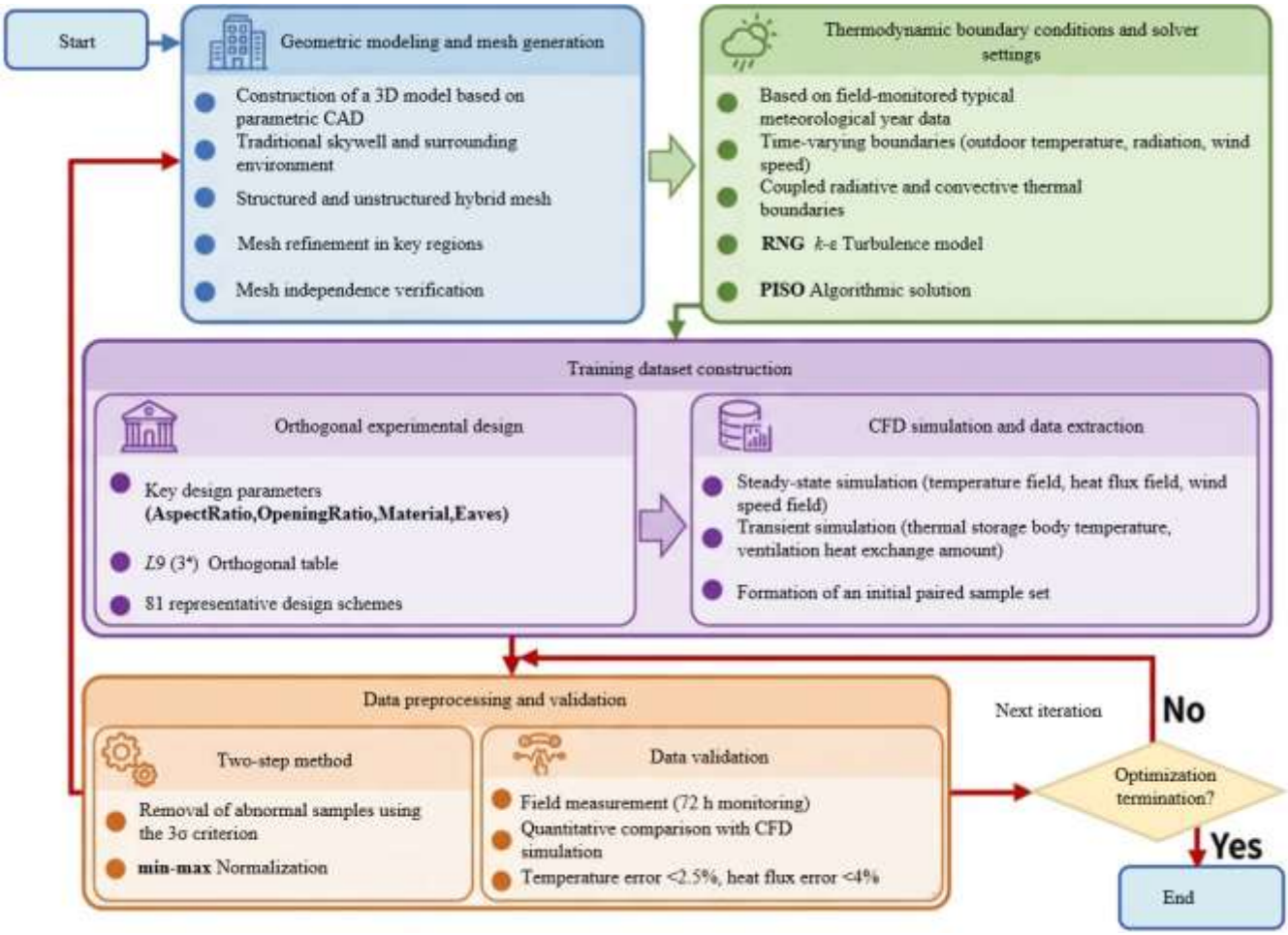

Figure 3. Flowchart of thermal environment simulation and training data construction for the traditional skywell

2.4 Quantitative indicator system for thermal environment regulation effects under relocation scenarios

To comprehensively quantify the thermal environment regulation effects of traditional skywells after relocation, a multidimensional quantitative indicator system is constructed based on thermodynamic mechanisms. This system covers three core dimensions: thermal regulation efficiency, thermal environment stability, and energy conservation. Each indicator has a clear thermodynamic physical meaning and a quantifiable calculation method. Thermal regulation efficiency indicators focus on the effectiveness evaluation of the core thermal regulation mechanisms of the skywell, including ventilation heat replacement efficiency, thermal storage efficiency, and radiative heat transfer suppression rate. The ventilation heat replacement efficiency η_v is defined as the ratio of the actual ventilation heat exchange to the theoretical maximum heat exchange, with the core formula given as:

$$\eta_v = \frac{m_a c_p \Delta T}{Q_s} \tag{17}$$

where, m_a is the ventilation mass flow rate, c_p is the specific heat capacity of air at constant pressure, ΔT is the temperature difference between inlet and outlet air, and Q_s is the total indoor heat gain. The thermal storage efficiency η_s is defined based on the energy balance principle as the ratio of the actual stored heat of the thermal storage body to the maximum storable heat, expressed as:

$$\eta_s = \frac{Q_{stare}}{\rho c V \Delta T_{\max}} \tag{18}$$

where, ρ, c, and V are the density, specific heat capacity, and volume of the thermal storage body, respectively, and ΔT_{max} is the maximum allowable temperature variation of the thermal storage body. The radiative heat transfer suppression rate η_r characterizes the shielding effectiveness of shading components against solar radiation and is calculated as:

$$\eta_r = \frac{q_{r0} - q_{r1}}{q_{r0}} \tag{19}$$

where, q_{r0} and q_{r1} are the radiative heat fluxes on the envelope surface without shading and with shading, respectively.

Thermal environment stability indicators focus on the thermal environment assurance capability under extreme climates, including extreme climate heat flux peak and

temperature fluctuation amplitude. The extreme climate heat flux peak q_{peak} is defined as the maximum absolute value of heat flux on the envelope surface during periods of extreme high temperature or cold waves, directly reflecting the resistance capability of the skywell to extreme thermal loads. The temperature fluctuation amplitude ΔT_v is defined as the difference between the maximum and minimum indoor temperatures within a typical day, quantifying the stabilizing regulation effect of the skywell on indoor temperature. Energy conservation indicators focus on the low-carbon benefits after relocation, including heat loss per unit area and passive thermal regulation contribution rate. The heat loss per unit area q_{loss} is defined as the total heat loss per unit area caused by indoor–outdoor heat exchange and is calculated as:

$$q_{loss} = \frac{\sum (q_i A_i)}{A} \tag{20}$$

where, q_i is the heat flux of each envelope structure, A_i is the corresponding area, and A is the total building footprint area. The passive thermal regulation contribution rate γ is defined as the ratio of the heat load reduced by passive thermal regulation to the total heat load, expressed as:

$$\gamma = \frac{Q_{tot} - Q_{pass}}{Q_{tot}} \tag{21}$$

where, Q_{tot} is the total heat load and Q_{pass} is the remaining heat load after passive regulation. This indicator system comprehensively covers the core thermodynamic characteristics of thermal environment regulation after the relocation of traditional skywells, providing a unified and precise quantitative benchmark for the performance evaluation of model-generated schemes.

3. EXPERIMENTAL DESIGN AND VALIDATION

The experimental design and validation take typical traditional skywell relocation as the carrier. Through precise scenario setting, systematic model performance evaluation, and multi-method comparison, the effectiveness and superiority of the thermodynamics-constrained cGAN method are comprehensively verified. Huizhou skywell dwellings are selected as the research object. The original morphological parameters are an aspect ratio of 1.6 and an opening ratio of 0.45. The envelope structure is mainly composed of traditional brick and stone and wood. The original thermodynamic characteristics are a summer ventilation heat replacement efficiency of 0.62 and a winter thermal storage efficiency of 0.71, which represent a typical example of passive thermal regulation of traditional southern skywells. Based on this, three types of relocation scenarios are set. The single-building relocation scenario is located in a new urban district, with spatial scale constraints of 70% of the original skywell area. The thermodynamic boundary conditions refer to local typical meteorological year data, with a summer outdoor temperature peak of 38℃ and a winter minimum of −2℃. The cluster relocation scenario is at the block scale and includes eight skywell units. The shading between buildings and mutual thermal radiation interactions are considered, and the boundary conditions superimpose the urban heat island effect, resulting in a 2℃ increase in the outdoor baseline temperature. The cross-climate-zone relocation scenario involves relocation from a southern humid region to a northern semi-arid region, with climate parameters adjusted to a 15% reduction in winter solar radiation intensity and a 20% increase in wind speed, and enhanced thermal insulation requirements for the envelope structure.

Model training is conducted based on the PyTorch deep learning framework, with the following training parameter settings: the AdamW optimizer is used, the initial learning rate is set to 1×10^{-4}, the learning rate is dynamically adjusted using a cosine annealing strategy, the number of iterations is 20000, the batch size is 32, and the weight decay coefficient is 0.001 to prevent overfitting. Model performance evaluation adopts a comprehensive system combining quantitative and qualitative analysis. Quantitative indicators include thermodynamic errors of generated parameters, thermal environment prediction accuracy, and generation efficiency. Qualitative analysis focuses on the compatibility of generated schemes with traditional morphology, which is judged by the degree of matching between core morphological parameters such as aspect ratio and opening ratio and those of traditional skywells. At the same time, a conventional cGAN model without thermodynamic constraints is introduced as a control. Through the performance differences between the two models, the key role of thermodynamic constraints in improving the physical credibility of generation results is verified.

To further highlight the advantages of the proposed method, three groups of comparative experiments are designed. The first group is the thermodynamics-constrained cGAN method proposed in this study, the second group is the traditional forward design method, and the third group is the conventional cGAN method without thermodynamic constraints. The comparison indicators cover three main dimensions. Design efficiency takes the number of iterations and computational time for single-scheme generation as the core, quantifying the optimization efficiency differences among different methods. Thermodynamic accuracy is measured by the prediction error of thermal environment indicators, evaluating the degree of agreement between the generated results and the real thermal environment. Scheme feasibility is determined by the combined compliance rate of traditional morphological compatibility and thermal performance compliance, where thermal performance compliance is based on the quantitative indicator system in Section 2.4, requiring ventilation heat replacement efficiency ≥0.55 and thermal storage efficiency ≥0.60. Through comprehensive comparison of the three methods, the overall advantages of the proposed method in efficiency, accuracy, and feasibility are systematically verified, providing data support for its engineering application.

4. RESULTS AND DISCUSSION

4.1 Model training results and performance analysis

Model training stability and overall performance are evaluated from multiple dimensions, including loss function convergence characteristics, thermodynamic errors, generation efficiency, and traditional morphological compatibility. The core quantitative results are shown in Table 1. As shown in Table 1, after 20000 training iterations, the thermodynamics-constrained cGAN model proposed in this study achieves stable convergence for all loss terms. The final converged values of adversarial loss, reconstruction loss, and thermodynamic consistency loss are 0.082, 0.056, and 0.031,

respectively, which are significantly lower than those of the conventional cGAN model without thermodynamic constraints. This indicates that embedding thermodynamic constraints effectively improves training stability and avoids oscillatory convergence behavior.

At the level of thermodynamic accuracy, the generated schemes produced by the proposed method exhibit an energy conservation residual of 2.3×10^{-4} J, a heat flux continuity residual of 1.2 W/m², and a root mean square error of temperature field prediction of 0.85℃. All of these results are significantly better than those of the unconstrained cGAN, with reductions exceeding 50%, confirming the key role of thermodynamic consistency loss in enforcing generated results to follow fundamental thermodynamic laws and substantially improving the physical credibility of model predictions. In terms of generation efficiency, the proposed method requires only 2.1 s to generate a single set of skywell design schemes, with 20000 iterations. Although the unconstrained cGAN has a similar number of iterations, the lack of thermodynamic constraints causes some schemes to require secondary validation, increasing the actual effective time to 3.5 s. In contrast, the traditional forward design method requires more than 120 s, highlighting the high efficiency advantage of the proposed method.

Analysis of traditional morphological compatibility shows that the core morphological parameters of skywells generated by the proposed method all fall within the typical parameter ranges of Huizhou traditional skywells, with a compatibility compliance rate of 100%. In contrast, in the schemes generated by the unconstrained cGAN, 35% of the samples exhibit aspect ratios deviating below 1.0 or above 2.0, and 28% of the samples have opening ratios lower than 0.3, resulting in a compatibility compliance rate of only 62%. These results indicate that, by embedding traditional morphological constraints, the proposed method achieves coordination between "thermal performance optimization" and "cultural inheritance," avoiding the tendency of generative models to deviate from traditional architectural morphological characteristics.

Table 1. Quantitative comparison of model training and performance

Evaluation Dimension	Specific Indicator	Proposed Method (Thermodynamics-Constrained cGAN)	cGAN Without Thermodynamic Constraints
Loss convergence characteristics	Final converged value of adversarial loss	0.082 ± 0.003	0.125 ± 0.006
	Final converged value of reconstruction loss	0.056 ± 0.002	0.089 ± 0.004
	Final converged value of thermodynamic consistency loss	0.031 ± 0.001	0.107 ± 0.005
Thermodynamic error	Energy conservation residual (J)	$2.3 \times 10^{-4} \pm 1.5 \times 10^{-5}$	$8.7 \times 10^{-4} \pm 3.2 \times 10^{-5}$
	Heat flux continuity residual (W/m²)	1.2 ± 0.15	3.8 ± 0.28
	Temperature field prediction RMSE (℃)	0.85 ± 0.06	1.62 ± 0.11
	Heat flux field prediction RMSE (W/m²)	2.1 ± 0.18	4.5 ± 0.32
Generation efficiency	Generation time per scheme (s)	2.1 ± 0.2	3.5 ± 0.3
	Iterations to stable convergence	20000 ± 500	19800 ± 620
Traditional morphology compatibility	Generated aspect ratio range	1.52 ~ 1.68	0.85 ~ 2.23
	Generated opening ratio range	0.42 ~ 0.48	0.22 ~ 0.71
	Proportion of traditional components (%)	85 ~ 92	68 ~ 95
	Morphological compatibility pass rate (%)	100	62

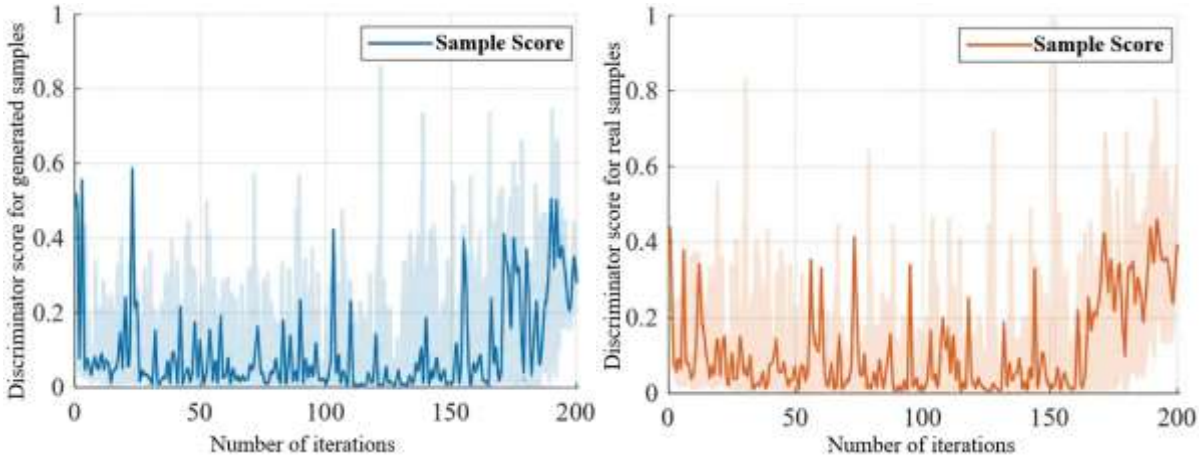

(1) Generated samples (2) Real samples

Figure 4. Variation of the discriminator comprehensive score (including thermodynamic consistency) for generated/real samples with iteration rounds

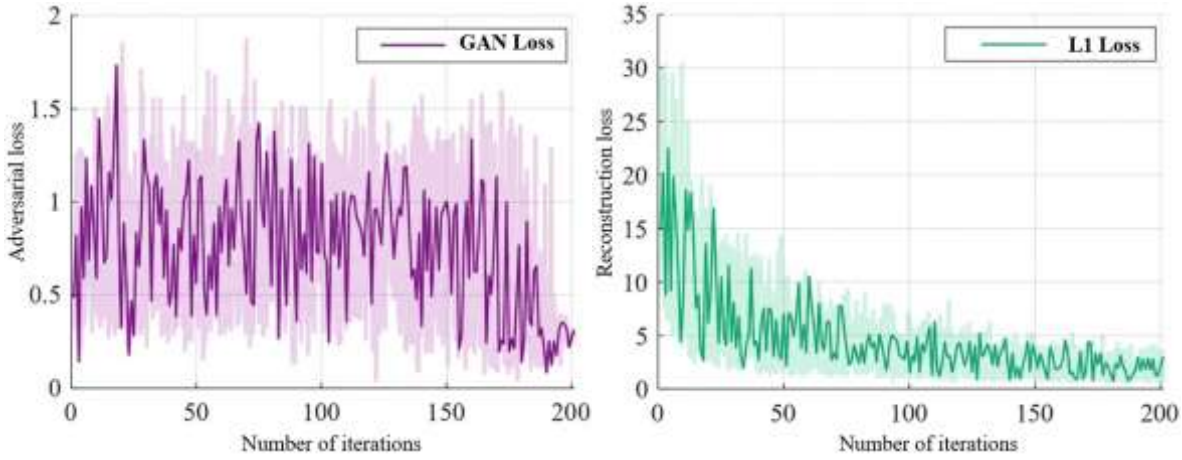

(1) Adversarial loss versus iteration rounds (2) Reconstruction loss versus iteration rounds

Figure 5. Loss iteration curves during training of the thermodynamics-constrained cGAN

To quantify the identification effectiveness of the discriminator in the thermodynamics-constrained cGAN on the "traditional skywell relocation design parameters–thermal environment data" samples in terms of "authenticity–thermodynamic compliance," it is necessary to analyze the temporal characteristics of its scoring for generated/real samples. As shown by the curves in Figure 4, during the first 50 iterations, the discriminator scores of generated samples fluctuate sharply (0–0.6), which is due to the generator not yet learning the core correlation features of traditional skywells, such as the coupling relationship between aspect ratio and stack-driven ventilation, and the matching rules between envelope materials and heat storage efficiency. After 50 iterations, the scores gradually stabilize in the range of 0.3–0.5, while the scores of real samples are consistently maintained in a higher range of 0.4–0.8, and the fluctuation ranges of both narrow synchronously. Further comparison shows that the overlap interval between the generated sample scores and the real sample scores expands with increasing iterations, indicating that the generated samples not only reproduce the morphological constraints of traditional skywells, but that their corresponding thermal environment data also satisfy the thermodynamic laws of the relocation scenarios. The experimental results confirm that the dual identification mechanism of the discriminator effectively screens generated samples that possess both traditional skywell morphological compatibility and thermodynamic rationality: it not only avoids the morphological distortion problem of "generated scheme aspect ratios deviating from traditional ranges" in unconstrained models, but also circumvents the physical violation problem of "thermal environment data violating energy conservation".

To analyze the collaborative mechanism of "adversarial game–target adaptation" during the training process of the thermodynamics-constrained cGAN, it is necessary to track the iterative evolution of adversarial loss and reconstruction loss to evaluate the fitting accuracy of the model to the thermal environment optimization objectives of traditional skywell relocation. As shown in Figure 5, the adversarial loss fluctuates significantly in the first 50 iterations, reflecting the game between the generator and the discriminator around the "reasonable distribution of traditional skywell relocation design," where the generator attempts to output design parameters that satisfy morphological constraints, and the discriminator identifies whether they match the thermodynamic correlations of real samples. After 50 iterations, the adversarial loss converges to the range of 0.5–1.0, indicating that both have reached a balance on the compliant distribution of "traditional skywell relocation design–thermal environment." The reconstruction loss rapidly decreases from above 20 in the initial stage and stabilizes at a low-loss range of about 5 at 200 iterations, corresponding to the continuous reduction of the deviation between the thermal environment indicators of the generated samples and the target values. Taking the single-building relocation scenario as an example, the deviation between the ventilation heat replacement efficiency of the generated scheme and the target value decreases from 15% in the initial stage to 2.1%, and the deviation of heat storage efficiency in the cross-climate-zone relocation decreases from 12% to 1.8%, both meeting the thermal performance accuracy requirements of relocation projects. The convergence characteristics of the curves indicate that the training process of the model achieves coordination between "adversarial game fitting the traditional skywell design distribution" and "reconstruction loss adapting to relocation thermal environment objectives": the adversarial loss ensures that the morphological and thermodynamic features of the generated schemes conform to the essential attributes of traditional skywells, while the reconstruction loss ensures precise matching to the thermal performance requirements of different relocation scenarios.

4.2 Simulation results of thermal environment regulation effects in different relocation scenarios

The quantitative results of core thermal environment regulation effect indicators for the three relocation scenarios and the original scenario are shown in Table 2. Combined with the analysis of temperature field, heat flux field distribution, and heat storage temperature temporal curves, the thermal regulation effects of skywells differ significantly under different scenarios. The optimized schemes generated by this method can effectively adapt to scenario constraints and improve thermal performance.

In the single-building relocation scenario, due to the reduction in spatial scale, the ventilation heat replacement efficiency of the original scheme decreases to 0.51, and the unit-area heat loss increases to 38.2 W/m². In contrast, the optimized scheme in this study, by slightly adjusting the opening ratio from 0.45 to 0.42 and extending the eaves length

to 1.2 m, achieves a ventilation heat replacement efficiency of 0.58 and a unit-area heat loss of 29.7 W/m², a reduction of 22.2% compared with the original relocation scheme. The temperature field simulation results indicate that the optimized scheme reduces the maximum summer temperature in rooms around the skywell by 2.3℃, and the heat flux field distribution is more uniform, with no local heat accumulation. Comparing the thermal differences between the original and single-building relocation scenarios shows that the limited spatial scale mainly weakens stack-driven ventilation intensity. The optimized scheme reconstructs the thermal stack ventilation path by adjusting the opening parameters and shading components, compensating for the thermal performance degradation caused by space reduction.

In the cluster relocation scenario, the eight skywell units generated by this method are arranged in a row-column layout, forming a 1.8 m wide cold alley system. Table 2 shows that the ventilation heat replacement efficiency in the cluster scenario reaches 0.63, an increase of 8.6% compared with the single-building scenario; the average temperature of the surrounding environment decreases by 1.5℃ compared with areas without cluster layout, and the uniformity of heat flux distribution improves by 35%, confirming the thermodynamic synergistic effect of cluster skywells. The cold alley system strengthens regional air circulation, accelerating heat diffusion, while the shading effect of adjacent skywells reduces envelope radiation heat flux, significantly mitigating the urban heat island effect, validating the applicability of this method in cluster layout optimization.

In the cross-climate-zone relocation scenario, the original scheme has insufficient heat storage, resulting in a winter heat storage efficiency of only 0.52 and a temperature fluctuation amplitude of 8.7℃ under extreme cold waves. The optimized scheme in this study increases wall thickness to 30 cm and adopts a composite envelope structure of traditional brickwork and modern insulation materials, raising the heat storage efficiency to 0.65 and reducing the temperature fluctuation amplitude under extreme cold waves to 5.2℃, with a passive thermal regulation contribution rate of 68%. Comparing the adaptation effects across different climate zones shows that relocation to northern regions requires prioritizing heat storage and insulation performance, while southern relocations focus on ventilation and heat dissipation optimization. This method can dynamically adjust design parameters according to climatic boundary conditions to generate adaptive schemes.

To quantify the passive thermal regulation performance of traditional skywell building clusters in modern cluster relocation scenarios and verify the synergistic thermal regulation effect of the traditional morphological elements "skywell–cold alley–water system," it is necessary to analyze the regional temperature field distribution during daytime in summer. From the thermal environment simulation visualization, the temperature of the external environment of surrounding buildings in the relocation area reaches 31.50℃, while the cold alley area inside the cluster decreases to 29.5℃, the skywell area maintains 30.20℃, and the area around the water system decreases to 28.5℃—the temperatures of the three types of traditional morphological spaces are respectively 2.0℃, 1.3℃, and 3.0℃ lower than the surrounding environment. This difference originates from the thermodynamic synergy of morphological elements: the narrow channel form of the cold alley strengthens airflow and accelerates heat diffusion; the water system directly reduces surrounding air temperature through latent heat of evaporation; the high aspect ratio (1.6) design of the skywell creates stack-driven ventilation, continuously transferring indoor heat to the cluster space.

Further analysis shows that the cluster layout of traditional skywell building clusters does not weaken the thermal regulation ability under modern relocation spatial constraints. Instead, through the spatial coupling of "skywell–cold alley–water system," a hierarchical thermal environment regulation system is formed: the water system as the core cold source reduces the local baseline temperature, the cold alley constructs ventilation corridors to transfer cool air, and the skywell enables heat exchange between individual buildings and cluster spaces. This result confirms that the morphological features of traditional skywells are thermodynamically compatible with the spatial requirements of modern cluster relocation. The synergistic mechanism of "morphological elements–thermal regulation performance" can directly guide the thermal environment optimization of relocation projects, preserving traditional architectural features while providing a passive technical pathway for mitigating local urban heat islands (Figure 6).

Table 2. Comparison of core indicators of thermal environment regulation effects under different scenarios

Scenario Type	Original Scenario	Single-Building Relocation (Before Optimization)	Single-Building Relocation (After Optimization)	Cluster Relocation (After Optimization)	Cross-Climate relocation (Before Optimization)	Cross-Climate Relocation (After Optimization)
Ventilation heat exchange efficiency	0.62 ± 0.03	0.51 ± 0.02	0.58 ± 0.02	0.63 ± 0.03	0.53 ± 0.02	0.56 ± 0.02
Thermal storage efficiency	0.71 ± 0.02	0.63 ± 0.02	0.68 ± 0.02	0.69 ± 0.02	0.52 ± 0.02	0.65 ± 0.02
Radiative heat transfer suppression rate (%)	42 ± 3	35 ± 2	48 ± 3	51 ± 3	32 ± 2	39 ± 2
Extreme heat flux peak (W/m²)	58.6 ± 2.5	65.2 ± 3.1	52.3 ± 2.2	49.8 ± 2.0	72.5 ± 3.5	56.4 ± 2.4
Temperature fluctuation amplitude (℃)	4.3 ± 0.4	6.5 ± 0.5	4.8 ± 0.4	4.1 ± 0.3	8.7 ± 0.6	5.2 ± 0.4
Heat loss per unit area (W/m²)	25.3 ± 1.8	38.2 ± 2.1	29.7 ± 1.6	24.8 ± 1.5	42.5 ± 2.3	31.2 ± 1.7
Passive thermal regulation contribution rate (%)	72 ± 4	55 ± 3	66 ± 3	73 ± 4	48 ± 3	68 ± 4

(1) Bird's-eye view

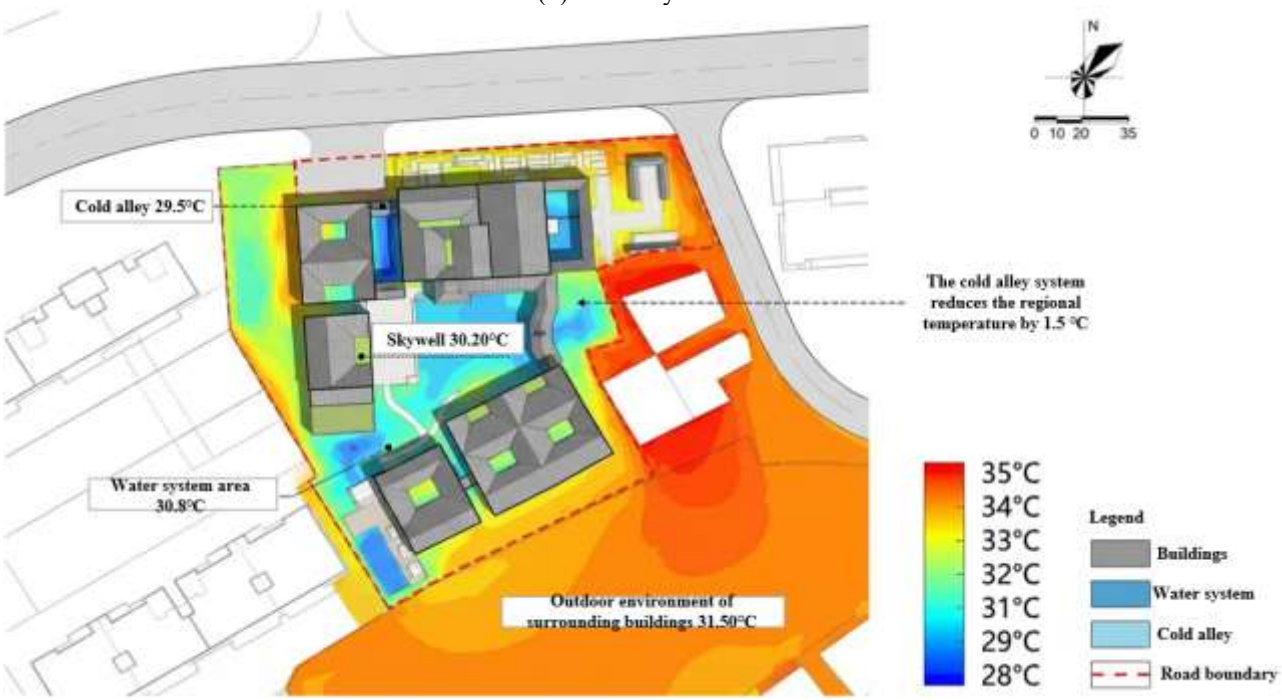

(2) Thermal environment simulation visualization

Figure 6. Summer daytime temperature field distribution of traditional skywell building clusters in the cluster relocation scenario

Table 3. Comprehensive quantitative comparison of overall performance for three groups of comparative experiments

Evaluation Dimension	Specific Indicator	Proposed Method	Traditional Forward Design Method	cGAN Without Thermodynamic Constraints
Design efficiency	Total computation time per scheme (s)	42 ± 3	6200 ± 280	486 ± 35
	Effective number of iterations	20000 ± 500	50 ± 8	20000 ± 620
	Improvement rate of single-scheme generation efficiency (%)	-	99.3	91.4
Thermodynamic accuracy	Temperature prediction error (%)	2.1 ± 0.3	4.8 ± 0.5	5.3 ± 0.6
	Heat flux prediction error (%)	3.2 ± 0.4	6.5 ± 0.7	7.8 ± 0.8
	Pass rate of energy conservation residual (%)	100	82	45
Scheme feasibility	Thermal performance pass rate (%)	95	68	52
	Traditional morphology compatibility pass rate (%)	100	85	62
	Overall feasibility pass rate (%)	95	58	32

4.3 Comparative experiment results analysis

The quantitative results of the comprehensive performance of the three comparative experiments are shown in Table 3. From the three dimensions of design efficiency, thermodynamic accuracy, and scheme feasibility, the superiority of this method is systematically verified.

In terms of efficiency, the total computation time for a

single optimal scheme using this method is only 42 s, with 20000 iterations; the traditional forward design method requires 50 rounds of parameter adjustments and CFD simulations, with a total time of 6200 s and 50 iterations. The computation time of this method is reduced by 99.3% compared with the traditional method, significantly improving engineering design efficiency. The unconstrained cGAN method generates a single scheme in 3.5 s, but due to insufficient thermodynamic consistency, an additional 12 rounds of secondary verification are required, increasing the total time to 486 s, still much higher than this method, indicating that thermodynamic constraints can avoid invalid iterations and improve design efficiency.

In terms of accuracy, the temperature prediction error of the scheme generated by this method is 2.1%, and the heat flux prediction error is 3.2%, both significantly lower than the traditional forward design and unconstrained cGAN. This result confirms that embedding thermodynamic constraints allows the generative model to learn the intrinsic thermodynamic relationship between design parameters and the thermal environment, improving prediction accuracy, while the traditional forward design relies on empirical parameter adjustments and the unconstrained cGAN lacks physical law constraints, both leading to insufficient accuracy.

In terms of feasibility, the thermal performance compliance rate of schemes generated by this method is 95%, the traditional morphology compatibility rate is 100%, and the overall feasibility compliance rate is 95%; the traditional forward design method has a thermal performance compliance rate of 68%, morphology compatibility rate of 85%, and overall compliance rate of 58%; the unconstrained cGAN has a thermal performance compliance rate of 52%, morphology compatibility rate of 62%, and overall compliance rate of only 32%. The comprehensive feasibility advantage of this method is significant, achieving coordinated compliance of "thermal performance–morphology–physical credibility," which better meets engineering application requirements.

4.4 Discussion of thermodynamic mechanisms and limitation analysis

Combining the quantitative results in Table 1, Table 2, and the simulation visualization data, the thermodynamic advantage of the optimal design scheme originates from the precise matching between the design parameters and the core thermal regulation mechanism of the skywell. The improvement of ventilation heat replacement efficiency is mainly achieved through the synergistic optimization of the opening ratio and eaves length: the opening ratio is adjusted from 0.45 to 0.42, reducing air circulation resistance, and the eaves are extended to 1.2 m, enhancing stack-driven ventilation power, increasing the thermal stack pressure difference between the skywell and rooms to 12 Pa, promoting air circulation and heat exchange. The optimization of heat storage performance is achieved by adjusting wall thickness and material combination. In the cross-climate relocation scenario, the 30 cm thick composite wall increases the specific heat capacity of the heat storage body to 1.8 kJ/(kg·℃), prolonging the heat release cycle and reducing the indoor temperature drop during winter nights by 3.5℃, meeting the insulation requirements of the semi-arid northern region. The increase of radiation heat transfer suppression rate is due to the optimized layout of shading components, reducing solar radiation heat flux on the envelope surface by 18%, decreasing indoor heat gain in summer.

The limitations of this method are mainly reflected in three aspects: First, the applicable boundary is limited. The current model is optimized only for urban relocation scenarios in plains areas. In relocation scenarios with complex terrain, the interference of terrain on wind fields and radiation is not included in the thermodynamic constraints, and model adaptability needs further verification. Second, objective sources of error exist. The CFD simulation uses the RNG k-ε turbulence model, which has limited simulation accuracy for low-speed airflow and does not consider the dynamic changes of material thermal properties, leading to slight errors in thermal environment prediction. Third, the refinement of morphology constraints is insufficient. Currently, only macro parameters such as aspect ratio and opening ratio are considered, while micro morphological features such as skywell decorative components and window/door styles are not included, which may affect the complete inheritance of traditional architectural features.

Future improvement directions can be carried out in three aspects: first, expand scenario adaptability by introducing terrain thermodynamic boundary conditions and constructing a multi-physics constraint model coupling terrain–wind field–radiation; second, improve mechanism modeling accuracy by developing a dynamic material thermal property update model, combined with long-term field monitoring data to optimize thermodynamic parameters; third, deepen morphology constraints by incorporating quantitative indicators of traditional skywell micro-morphological features, realizing synergistic optimization of "macro performance–micro morphology." In addition, human-building coupled thermodynamic analysis can be introduced, incorporating indoor thermal comfort indicators into the objective function to enhance the human-oriented design level of the scheme.

5. CONCLUSIONS AND OUTLOOK

This study addressed the thermal environment adaptability problem in the modern relocation of traditional skywells and proposed a thermodynamics-constrained cGAN inverse generation method. Through systematic experiments and mechanism analysis, the core conclusions are as follows: The thermodynamics-constrained cGAN model demonstrated excellent training stability, with final converged values of adversarial loss, reconstruction loss, and thermodynamic consistency loss being 0.082, 0.056, and 0.031, respectively. The generated schemes exhibited energy conservation residuals and heat flux continuity residuals of only 2.3×10^{-4} J and 1.2 W/m², significantly outperforming the conventional cGAN model without thermodynamic constraints. This method achieved synergistic optimization of thermal performance and traditional morphology across three relocation scenarios. In the single-unit relocation, ventilation heat replacement efficiency was improved to 0.58; in the cluster relocation, the cold alley system reduced the surrounding environment temperature by 1.5℃; in the cross-climate relocation, temperature fluctuation under extreme cold waves was reduced to 5.2℃. Results of three comparative experiments show that this method reduced computation time by 99.3% compared with traditional forward design, improved thermodynamic prediction accuracy by more than 50% compared with the unconstrained cGAN, and achieved a comprehensive feasibility compliance rate of 95%, far

exceeding the other two comparative methods. These experimental results fully verified the effectiveness and superiority of embedding thermodynamic constraints into the generative model, providing a reliable technical pathway for optimizing the thermal environment of traditional skywell relocations.

The academic contribution and engineering significance of this study are remarkable. Academically, it constructs an interdisciplinary research framework of "traditional building thermal regulation mechanism–generative model–inverse design," overcoming the limitation of conventional generative models lacking physical mechanism constraints, enriching the theory system of thermodynamics-driven architectural design optimization, and providing a new academic research paradigm for the adaptive reuse of traditional architectural heritage. From an engineering perspective, the proposed method provides precise and efficient thermal environment optimization solutions for traditional skywell relocation projects, addressing the core problem of imbalance between traditional morphology and modern thermal requirements during relocation. Its quantified thermal environment regulation indicators and scenario adaptation strategies can directly guide relocation project practice, offering key technical support for the revitalization of traditional architectural heritage and low-carbon urban construction, contributing to the achievement of the "dual carbon" goals in the building sector.

ACKNOWLEDGEMENTS

This paper was supported by the Major projects of natural science of the Education Department in Anhui province (Grant No.: 2023AH040183); 2023 Open Topics in the Key Laboratory of Huizhou Architecture in Anhui Province (Grant No.: HPJZ202304); the Key projects of humanities and social sciences of the Education Department in Anhui province (Grant No.: SK2020A0464); Anhui Provincial Cultural and Tourism Scientific Research Project (Grant No.: WL2023YB07).

REFERENCES

[1] Piotrowska-Woroniak, J., Cieśliński, K., Woroniak, G., Bielskus, J. (2022). The impact of thermo-modernization and forecast regulation on the reduction of thermal energy consumption and reduction of pollutant emissions into the atmosphere on the example of prefabricated buildings. Energies, 15(8): 2758. https://doi.org/10.3390/en15082758

[2] Nabil, M., Mahri, Z.L. (2022). Assessment of the 2016 thermal regulation for an Algerian building. Case study: Impact of window type, orientation and opening ratio on energy load using TRNSYS. Russian Journal of Building Construction and Architecture, 4: 7-17. https://doi.org/10.36622/vstu.2022.56.4.001

[3] Chan, A.L. (2023). Evaluating the appropriateness of adopting a single Overall Thermal Transfer Value and its implication to building energy regulation. Journal of Building Engineering, 76: 107225. https://doi.org/10.1016/j.jobe.2023.107225

[4] Seddik Hassan, A.M., Abd El Aal, R.F.A., Fahmi, A.A.E., Ali, S.M.A., Abdelhady, M.I. (2024). Courtyard geometry's effect on energy consumption of AlKharga city residential buildings, Egypt. Scientific Reports, 14(1): 11149. https://doi.org/10.1038/s41598-024-60487-8

[5] Tabesh, T., Sertyesilisik, B. (2016). An investigation into energy performance with the integrated usage of a courtyard and atrium. Buildings, 6(2): 21.

[6] Al Haddad, M., Al Shawabkeh, R., Arar, M., Rjoub, A., Alhammad, R., Senouci, A., Maherzi, W. (2024). Modeling the role of courtyards with clusters of buildings in enhancing sustainable housing designs. Buildings, 14(7): 2088. https://doi.org/10.3390/buildings14072088

[7] Taleghani, M., Tenpierik, M., van den Dobbelsteen, A. (2012). Environmental impact of courtyards—A review and comparison of residential courtyard buildings in different climates. Journal of Green Building, 7(2): 113-136.

[8] Gonzalez-Redondo, E. (2021). Timber-framed courtyard buildings: Construction, transformation and conservation of houses, inns and collective courtyard buildings. Informes de la Construcción, 73(563): 1-6.

[9] Ren, D.M., Yang, C., Xu, G.H. (2021). A study of aerial courtyard of super high-rise building based on optimisation of space structure. Applied Mathematics and Nonlinear Sciences, 6(2): 65-78.

[10] Yaşa, E., Ok, V. (2014). Evaluation of the effects of courtyard building shapes on solar heat gains and energy efficiency according to different climatic regions. Energy and Buildings, 73: 192-199. https://doi.org/10.1016/j.enbuild.2013.12.042

[11] Wang, A., Wang, H. (2022). Analysis of the thermal performance of external insulation in prefabricated buildings using computational fluid dynamics. Fluid Dynamics and Materials Processing, 18(5): 1293-1306. https://doi.org/10.32604/fdmp.2022.018561

[12] Vasudevan, M., Basu, B., Pilla, F., Mcnabola, A. (2022). Development and validation of a computational fluid dynamics modelling methodology for isolated and urban street canyon configurations using wind tunnel measurements. International Journal of Computational Methods and Experimental Measurements, 10(2): 104-116. https://doi.org/10.2495/CMEM-V10-N2-104-116

[13] Zeng, X.R., Zhang, J.H., Li, L.M., Zuo, J.X. (2024). Enhanced design of piston cooling nozzles via computational fluid dynamics. Power Engineering and Engineering Thermophysics, 3(1): 45-57. https://doi.org/10.56578/peet030104

[14] Riahinezhad, L., Mohammadkhah, M., Nooraeen, A. (2025). Analysis of ventilation architectures for data center cooling using steady and transient computational fluid dynamics simulations. Mathematical Modelling for Sustainable Engineering, 1(1): 48-62. https://doi.org/10.56578/mmse010104

[15] Wang, J. (2024). Thermal comfort simulation in furniture design: Integrating considerations of the building thermal environment. International Journal of Heat & Technology, 42(2): 688-696. https://doi.org/10.18280/ijht.420236

[16] Li, B., Guo, W., Liu, X., Zhang, Y., Russell, P.J., Schnabel, M.A. (2021). Sustainable passive design for building performance of healthy built environment in the Lingnan area. Sustainability, 13(16): 9115. https://doi.org/10.3390/su13169115

[17] Liu, Y., Yang, L., Hou, L., Li, S., Yang, J., Wang, Q. (2017). A porous building approach for modelling flow

and heat transfer around and inside an isolated building on night ventilation and thermal mass. Energy, 141, 1914-1927. https://doi.org/10.1016/j.energy.2017.11.137

[18] Contreras-Cruz, M.A., Correa-Tome, F.E., Lopez-Padilla, R., Ramirez-Paredes, J.P. (2023). Generative Adversarial Networks for anomaly detection in aerial images. Computers and Electrical Engineering, 106: 108470. https://doi.org/10.1016/j.compeleceng.2022.108470

[19] Xue, Y., Tong, W., Neri, F., Chen, P., Luo, T., Zhen, L., Wang, X. (2023). Evolutionary architecture search for generative adversarial networks based on weight sharing. IEEE Transactions on Evolutionary Computation, 28(3): 653-667. https://doi.org/10.1109/TEVC.2023.3338371

[20] Edalatifar, M., Shafi, J., Khalid, M., Baro, M., Sheremet, M.A., Ghalambaz, M. (2024). An artificial intelligence approach for the estimation of conduction heat transfer using deep neural networks. International Journal of Numerical Methods for Heat & Fluid Flow, 34(8): 3107-3130. https://doi.org/10.1108/HFF-11-2023-0678